Article

The Optimization of a First-Stage Liquid-Sealing Impeller Structure for a Turbopump Based on Response Surface Methodology

Qiong Liu [1], **Suguo Zhuang** [2], **Haifeng Bao** [3], **Zhoufeng He** [3], **Kai Wang** [3,*] and **Houlin Liu** [3]

1   Institute of Science and Technology Information, Jiangsu University, Zhenjiang 212013, China
2   School of Mechanical Engineering, Northwestern Polytechnical University, Xi'an 710072, China
3   Research Center of Fluid Machinery Engineering and Technology, Jiangsu University, Zhenjiang 212013, China
*   Correspondence: wangkai@ujs.edu.cn

Abstract: This study investigated the sealing performance of the multistage liquid-sealing impellers of a turbopump. To achieve this purpose, the influence of each structural parameter in the impeller on the pressurization coefficient φ^2 and the leakage flow rate Q was analyzed based on response surface methodology, taking the maximum pressurization coefficient φ^2 and the minimum leakage flow rate Q as the optimization objectives. We obtained satisfactory ranges for parameters φ^2 and Q. A set of parameter combinations was selected as the optimization scheme using the Box–Behnken method for the optimal solution design. The numerical simulation results show that to keep φ^2 and Q in the better range, the value ranges of groove width b, groove depth h and groove number z should be (12.8–14 mm), (4.5–5.6 mm) and (23.5–28), respectively. Compared with the original model, the optimized version has an average increase of about 2.5% in pressurization coefficient φ^2 at each rotation speed, an average of about 8.2% reduction in the leakage flow rate Q in the leakage state and an average increase in the reverse flow rate Q by about 6.7% in the negative pressure sealing state, indicating better sealing. By comparing pressure data at the experimental monitoring points, the proposed method was verified to have a high degree of confidence.

Keywords: first-stage liquid-sealing impeller; turbopump; response surface methodology; structural optimization

1. Introduction

As one of the important components of a liquid rocket motor system, the seal plays a key role in the safe and stable operation of a rocket. With the development of liquid rocket engines towards high performance, large variable ratios, multiple starts and repeated use, higher performance and reliability requirements have been placed on sealing devices. As a non-contact sealant, liquid-sealing impeller can be a good solution to the current problem of abrasion loss efficiency or high leakage on the sealing face of liquid oxygen turbopumps for rocket engines.

In 1959, Wolf [1] conducted a study on rocket turbopump seals and pointed out the need for turbopump seals including the four necessary seals in turbopump: oxidiser seals, fuel seals, gas seals and oil seals. The oxidiser seal is mainly a face seal with sealing properties developed over the last decade. In 1979, Masataka Nosaka [2] developed a seal for a liquid hydrogen turbopump to match the 10-ton thrust hydrogen–oxygen rocket engine being developed in Japan for launching large artificial satellites and successfully tried out a mechanical seal with low leakage, stable sealing performance, low starting torque and meeting lifetime requirements. At the same time, a trial production test of the floating ring seal was carried out to verify the stable leakage characteristics. Zhang [3] introduced the common rotary shaft seals in liquid rocket engine turbopump, including the labyrinth seal, end face seal, lip seal, floating ring seal and other basic seal forms. The

author pointed out that the radial gap is a controllable seal or labyrinth seal that can meet the requirements of pressure, velocity, temperature and life, but the leakage is not suitable for adoption. A new design principle and structure had to be adopted to meet all the requirements for the rotating shaft seal of the main engine turbopump of the space shuttle, that is, hydrostatic or hydrodynamic seal. Dirusso [4] studied a spiral groove dry gas seal for turbopumps and analyzed the lift characteristics of the spiral groove. The results show that by optimizing the design of the spiral groove, enough lift can be generated to make the seal operate in a non-contact state within the working range. Du [5] systematically studied the design structure of a high-pressure liquid rocket motor seal to improve the working reliability of the device. Under the condition of reliable operation in high-pressure sealing, they proposed a new sealing structure that should be adopted, a self-tightening structure, and designed dozens of seal structures. Through the test screening, 12 new seal structures were obtained. The experiment proved the reliable performance of the new seal structure, and the structure has been widely applied in many engines. Huang et al. [6] conducted a study of floating seals for ultra-high-speed pumps in liquid rocket engines. They proposed the working mode of floating rings and determined both the calculation method of minimum liquid film thickness and leakage volume and the issues that should be focused on in the process of structural design and product production. Lee et al. [7] proposed a floating ring seal with bump foil and with bump thicknesses of 0.076, 0.1 and 0.12 mm and separately tested these for pressure drops of 3.0, 5.0 and 7.0 MPa with rotor speed up to 24,800 rpm. The measured data included leakage performance, attitude angle, eccentric lock-up ratio and rotordynamic coefficients such as stiffness, damping and equivalent whirl frequency ratio to decide the whirling stability of the seal were compared with the floating ring seal. Huang [8] analyzed the three-dimensional flow characteristics in the labyrinth seal of a liquid hydrogen turbopump by numerical method, constructed the dynamic model of the labyrinth seal system of the turbopump rotor and analyzed the stability of the system and its influence law. Zhang et al. [9] studied non-contact sealing technology, analyzed its current status in rocket engine turbopump rotary shaft sealing and concluded that dry gas sealing and dynamic-static hybrid sealing could be applied to liquid rocket engine turbopumps. Zhao et al. [10] proposed the design idea of using a hybrid dynamic–static seal to solve the abrasion problem of the face seal of liquid oxygen pumps for liquid oxygen/kerosene rocket engines and studied the key technology to give the general selection principles of hybrid seal liquid film seal and gas film seal. Zhuang et al. [11] studied the effect of floating ring seal eccentricity on film thickness and pressure distribution. They conducted theoretical calculations and simulation analysis of flow characteristics for three structures, an ordinary floating ring, labyrinthine floating ring and fluid dynamic pressure ring flap-type floating ring. The results showed that labyrinthine floating rings and fluid dynamic pressure ring flap-type floating rings were significantly better than ordinary floating rings in terms of leakage and interstitial fluid velocity. Wei et al. [12] studied the face seal of a liquid rocket engine turbopump, proposed a method of calculating the disengagement pressure based on the elastic test value theory, researched an integrated disengagement test control technology and used an automated disengagement test system to test and verify the theoretical calculation results. The results showed that the theoretical calculation method and the automated disengagement test technology were accurate and feasible, which improved the stability and reliability of the end face seal of the test data and could effectively ensure the working performance and life of the liquid rocket engine. Xu et al. [13] investigated the lubrication performance and stability improvement of rocket turbopump mechanical seals by attaching superconducting magnetic force and presented a comprehensive multiphysics numerical model including microscale clearance flow and magnetic field as well as three degrees of freedom dynamic motion. Zhuang et al. [14] carried out unsteady numerical simulations of the liquid-phase conditions of the first-stage liquid-sealing impeller of a liquid oxygen turbopump. They analyzed the effect of rotational speed on the internal flow field and sealing characteristics of the first-stage liquid-sealing impeller.

In summary, most of the research on turbopump seals focused on mechanical seals. The extant literature did not test the forms of seals, such as centrifugal seals, especially for their structural optimization. Therefore, to improve their sealing performance, the influence of each structural parameter in the first-stage liquid-sealing impeller of a turbopump on the pressurization coefficient and the leakage flow rate was analyzed in this study based on the response surface methodology, taking the maximum pressurization coefficient and the minimum leakage flow rate as the optimization objectives.

2. Research Model and Structural Optimization Method Based on the Response Surface Methodology

2.1. Research Model

The multistage liquid-sealing impeller of the liquid oxygen turbopump (Figure 1) studied in this paper shows the sealing effect by reducing the pressure of the fluid medium step by step through the circumvolution of two centrifugal sealing impellers. The study in this paper is in a state where the decoupling seal has been opened, and the end face seal behind the second-stage liquid-sealing impeller is considered fully sealed [14]. The calculation model and details of the first-stage liquid-sealing impeller are shown in Figure 2, and its structural parameters are shown in Table 1. The work is completely computational using CFD (Fluent) techniques. The hexahedral mesh is used in the calculation, and the corresponding prism layer is set on the wall to capture the boundary layer. The overall index of Y+ is less than 5.
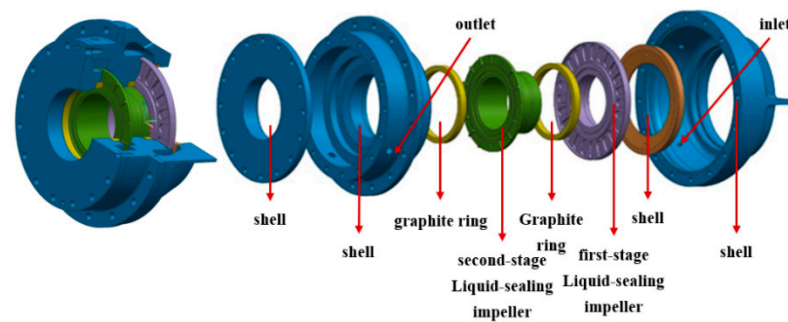

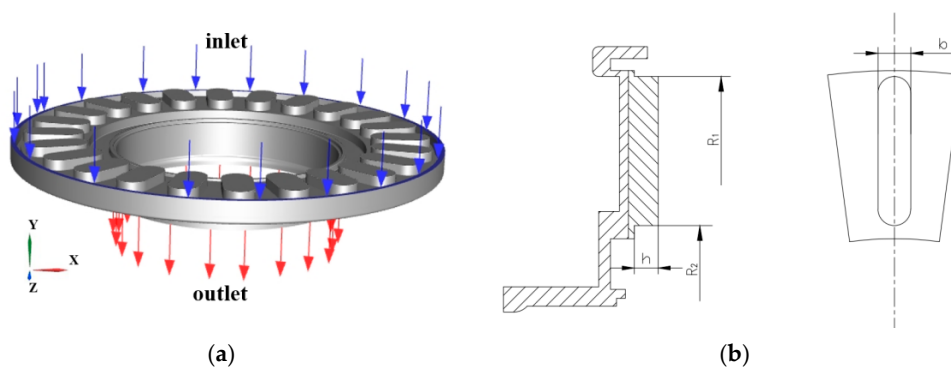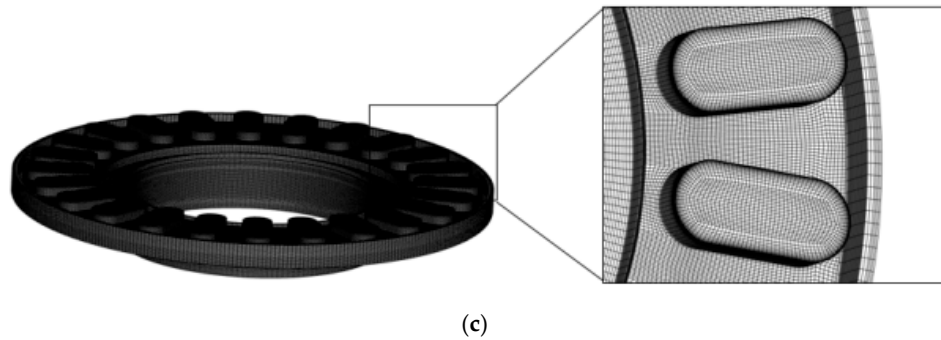**Figure 1.** Three-dimensional model of multistage liquid-sealing impellers.

(**a**)   (**b**)

Figure 2. *Cont*.

(**c**)

Figure 2. Computational domain of flow field in the first-stage liquid-sealing impeller. (**a**) Computational domain; (**b**) Location distribution of structural parameters (Table 1); (**c**) Meshing.

Table 1. Main structural parameters of the first-stage liquid-sealing impeller.

Number	Structural Parameters	Symbol	Numerical Value
1	Groove inner diameter/mm	R_1	60
2	Groove outside diameter/mm	R_2	85
3	Groove width/mm	b	12
4	Groove depth/mm	h	4
5	Groove number	z	24

2.2. Basic Ideas

The response surface method (RSM) was first proposed by Box and Wilson [15] to address the problem of optimal conditions in chemical research. Initially, the response surface method was mainly used in the chemical industry. The main idea was to establish an approximate function between the design objective and the design parameters through a certain experimental design method. Since the approximation function is a surface in N-dimensional space, it is known as response surface methodology. Because the response surface method can obtain the relationship between design objectives and design parameters with a smaller test scale, shorter test period and lower test cost, it has been widely applied in engineering optimization.

The response surface methodology of optimization is divided into three main steps: (1) determination of design parameters and their levels; (2) design of experiments and prediction and verification of schemes with the help of software platforms such as Design Expert; and (3) obtaining response surface graphs with the help of software platforms such as Design Expert and establishing an approximate functional relationship between design objectives and design parameters through the response surface graphs to finally obtain the best combination of design parameters.

2.3. Experimental Design

2.3.1. Design Parameters and Optimization Objectives

It can be seen from the empirical equations in the literature [14] that previous studies have often neglected the influence of groove number z, groove width b and groove depth h on the sealing performance of the centrifugal sealing impeller, where the optimization of these three structural parameters does not increase the axial and radial dimensions of the liquid-sealing impeller and can meet the spacecraft's requirements for minimizing the volume and weight of the components. Therefore, in this paper, the groove width b, groove depth h and groove number z are taken as design parameters in the response surface optimization test design of the first-stage liquid sealing impeller. The optimization objectives are to maximize the pressurization capacity and minimize the leakage flow rate

to explore the rules of their influence on the pressurization coefficient and leakage flow rate of the first-stage liquid sealing impeller.

As an important optimization index in this paper, the pressurization coefficient refers to the ratio between the actual pressurization value ΔP and the theoretical pressurization value ΔP_t, which can be calculated by Formulas (1) and (2) [14]. The two parameters are equal in theory, but in actual work, due to the gap between the impeller and the cavity, the viscosity of the liquid in the sealed cavity and other factors, the actual pressurization is lower than the theoretical pressurization. The pressurization coefficient can be calculated by Formula (3):

$$\Delta P = P_2 - P_1 \tag{1}$$

$$\Delta P_t == \frac{1}{2}\rho\omega^2\left(R_2^2 - R_1^2\right) \tag{2}$$

$$\varphi^2 = \frac{\Delta P}{\Delta P_t} \tag{3}$$

where ρ is the density of the fluid medium, (kg/m^3); ω is the rotating angular velocity of the impeller, (rad/s); R_1 is the inner diameter of the impeller, (mm); R_2 is the outer diameter of the impeller, (mm); P_1 is the pressure at the bottom of the groove; and P_2 is the pressure at the top of the groove.

The design flow chart of the response surface methodology for optimizing the first-stage liquid-sealing impeller is shown in Figure 3.
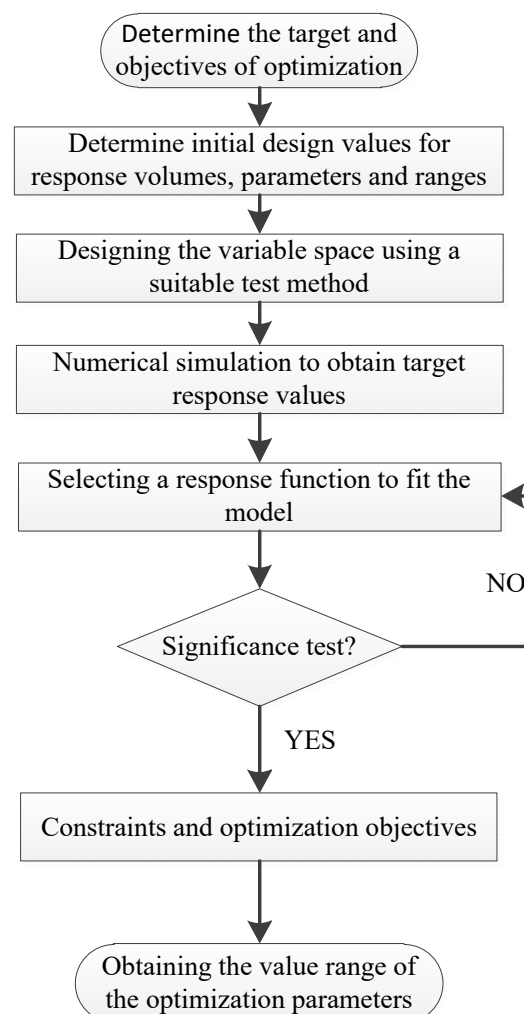
Figure 3. Design flow chart of the response surface method.

Each design parameter in the experimental design was set to three levels, -1, 0, and 1. In order to solve the problem of different design parameter scales and design parameter ranges, the range of variation of the design parameters was set to between -1 and 1. The design parameters were first changed by coding, which means that the design parameters were changed linearly. The main process is as follows:

(1) Let the constraint range of the i'th design parameter x_i be $[x_{1i}, x_{2i}]$ ($i = 1, 2, \ldots, m$), then the centroid of the constraint range is $x_{0i} = \frac{x_{1i}+x_{2i}}{2}$, and the radius length is $\Delta i = \frac{x_{2i}-x_{1i}}{2}$ ($i = 1, 2, \ldots, m$), and the linear transformation shown in Equation (4) is performed.

$$z_i = \frac{x_i - x_{0i}}{\Delta i} (i = 1, 2, \ldots, m) \tag{4}$$

(2) After the above transformation, the design parameter x_i change interval is transformed to $(-1, 1)$. Thus, the design parameter region shaped like a rectangle is transformed into a cube region centered at the origin. After encoding and transformation, the design parameters are shown in Table 2.

Table 2. Design parameters and levels.

Design Parameters	Code	Code Level		
		-1	0	1
Groove width b (mm)	x_1	8	11	14
Groove depth h (mm)	x_2	2	4	6
Groove number z	x_3	16	22	28

2.4. Design of Experimental Schemes

The accuracy of the response surface relies on the distribution of sampling points in the design space, so the design of the test is critical; certain selection guidelines need to be followed when choosing sample points to achieve high accuracy of the response function with a smaller number of points. Common test design methods include central composite design and Box–Behnken design. The central composite design is more suitable for experiments with multiple design parameters and coding levels to fit the response function more accurately. Still, compared with the Box–Behnken design, the central composite design has a larger test size and is less efficient and more costly to optimize [16]. Box–Behnken designs are more widely used in studies with fewer design parameters and coding levels. They have a smaller test size than the central composite in studies of optimized designs with three or four variables [17]. Therefore, they has higher optimization efficiency and lower test costs for an accurate fit to the optimization objective.

In this paper, the Box–Behnken design method is used to optimize the design of the experimental scheme. Using the experimental design software Design Expert 10.0 (Stat-Ease Inc. Minneapolis, MN, USA), 17 sets of schemes were obtained according to the Box–Behnken design method as shown in Table 3. Among them, the first 12 groups of test points were analysis points, and the last 5 groups were test center points. Multiple groups of experimental centers were set to improve the accurate estimation of simulation errors and ensure that there were sufficient degrees of freedom for analyzing experimental errors.

Table 3. Test scheme design.

Scheme	Variable		
	b (mm)	*h* (mm)	*z*
Y1	−1	−1	0
Y2	1	−1	0
Y3	−1	1	0
Y4	1	1	0
Y5	−1	0	−1
Y6	1	0	−1
Y7	−1	0	1
Y8	1	0	1
Y9	0	−1	−1
Y10	0	1	−1
Y11	0	−1	1
Y12	0	1	1
Y13	0	0	0
Y14	0	0	0
Y15	0	0	0
Y16	0	0	0
Y17	0	0	0

2.5. Numerical Simulation Calculations for Each Test Scheme

Each test scheme was modeled and meshed. Numerical simulations were carried out to calculate the unsteady flow field in the first-stage liquid-sealing impeller at the rotational speed of 10,000 rpm and inlet pressure of 3 MPa.

Figure 4 shows the results of the grid independence analysis of the first-stage liquid-sealing impeller. When the efficiency and accuracy of the calculation were taken into account, when the total number of grids reaches 2,754,456, the pressure became stable, and further increases in the total number of grids had no significant effect on the calculation results; therefore, a grid scheme with a total of 2,754,456 grids was chosen for the numerical optimization of the first-stage liquid-sealing impeller.
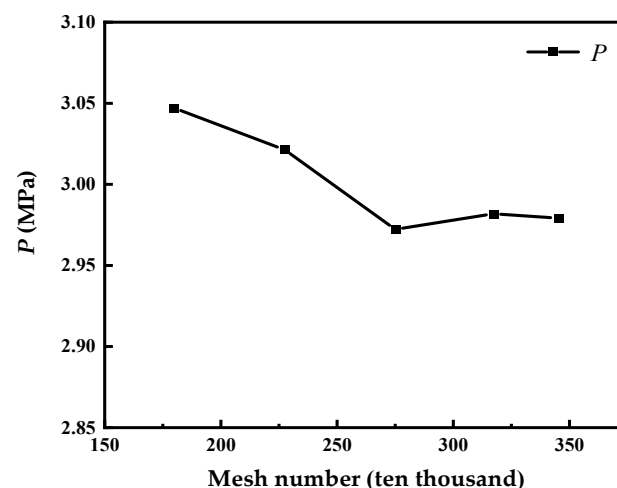
Figure 4. Grid independence analysis.

In calculating transient problems, the time step is particularly important for the stability of calculation and the accuracy of calculation results. When the time step is too large, it will lead to deviation in the calculation results. If the time step is too small, it will lead to a decline in the calculation efficiency. In the same node scheme and the same time step, the flow field pressure parameters at different loop positions are different. Table 4

shows pressure detection points at the same location under typical working conditions. Finally, we selected the time step as 4°.

Table 4. Time-step sensitivity analysis.

Rotation Angle/Step	Δt/s	Pressure (MPa)
0.5°	8.3333×10^{-6} s	2.97895
1°	1.6667×10^{-5} s	2.98158
2°	3.3333×10^{-5} s	2.97194
4°	6.6667×10^{-5} s	2.98163
8°	1.3333×10^{-4} s	3.04696

The numerical calculation method for the grid of the first-stage liquid-sealing impeller is the same as in the literature [13]. SST k–ω was chosen for the turbulence model, and the pressure inlet boundary condition and the pressure outlet boundary condition were used for the inlet and outlet boundary conditions of the calculation domain. In actual work, the inlet pressure of the liquid-sealing impeller is 3 MPa, which is obtained according to the test, and the outlet is atmospheric pressure. Table 5 shows the basic setup for the numerical simulation of the first-stage liquid-sealing impeller.

Table 5. Boundary conditions and calculation settings.

	Project	Type	Numerical Value
Boundary Condition Settings	Inlet boundary condition	Pressure inlet	3 MPa (total pressure)
	Outlet boundary condition	Pressure outlet	0.1 MPa
	Impeller steering/speed	Y axis	10,000 rpm
	Project	**Numerical Value**	
Solve Control	Time Step	6.6667×10^{-5} s (Solve every 4°, determined according to actual working conditions)	
	Convergence residuals	1×10^{-4}	
	The maximum number of iterations	20	
	Calculated number of revolutions	20 r	
	Reference pressure	0 MPa	

In this paper, numerical calculations are performed using ansys fluent2020R2 (Ansys Inc., Pittsburgh, PA, USA).The wall boundary condition chosen was no-slip wall. A pressure-velocity coupling-based solver was used. The gradient and pressure were discrete least squares cell based and PRESTO!, respectively. In addition, the first-order upwind mode was used as a discrete residual term, and the default parameters were used for each relaxation factor.

3. Results and Analysis

3.1. Results Analysis of Response Surface Optimization for the Pressurization Coefficient

3.1.1. Parameter Significance Analysis

The pressurization coefficient φ^2 of the first-stage liquid-sealing impeller under each scheme is shown in Table 6.

Table 6. Numerical simulation results of the pressurization coefficient.

Scheme	Y01	Y02	Y03	Y04	Y05	Y06
φ^2	0.648115	0.716191	0.806629	0.807534	0.800714	0.757505
Scheme	**Y07**	**Y08**	**Y09**	**Y10**	**Y11**	**Y12**
φ^2	0.80373	0.809979	0.566656	0.80551	0.663922	0.813344
Scheme	**Y13**	**Y14**	**Y15**	**Y16**	**Y17**	
φ^2	0.804388	0.804388	0.804388	0.804388	0.804388	

Based on Design Expert 10.0, response surface methodology was fitted to the numerical simulation results, and the regression equation for pressurization coefficient φ^2 of the first-stage liquid-sealing impeller was obtained as follows:

$$\varphi^2 = 0.62824 - 0.027193x_1 + 0.16444x_2 - 0.01143x_3 + 0.00086x_1x_2 + \\ 0.00036x_1x_3 + 0.00051x_2x_3 + 0.00073x_1{}^2 - 0.01872x_2{}^2 + 0.00017x_3{}^2 \tag{5}$$

where x_1 is the groove width, x_2 is the groove depth, x_3 is the groove number, x_1x_2 is the interaction term of groove width and depth, x_1x_3 is the interaction term of groove width and number, and x_2x_3 is the interaction term of groove depth and number.

The significance test of the regression equation coefficient and reliability analysis of the response surface model are shown in Tables 7 and 8, respectively.

Table 7. Significance test of regression equation coefficient of the pressurization coefficient.

Factor	Sum of Square	Degree of Freedom	Mean Square	Standard Deviation	F	Prob (P) > F	Significance
Model	0.066	9	0.0072823	0.005903	41.8	<0.0001	significant
x_1	0.0000066	1	0.0000066	0.004667	0.038	0.8512	Not significant
x_2	0.04	1	0.04	0.004667	229.5	<0.0001	significant
x_3	0.00147	1	0.00147	0.004667	8.43	0.0228	Secondary significant
x_1x_2	0.0001075	1	0.0001075	0.0066	0.62	0.4579	Not significant
x_1x_3	0.0001725	1	0.0001725	0.0066	0.99	0.3528	Not significant
x_2x_3	0.0001475	1	0.0001475	0.0066	0.85	0.388	Not significant
$x_1{}^2$	0.0001807	1	0.0001807	0.006433	1.04	0.3424	Not significant
$x_2{}^2$	0.024	1	0.024	0.006433	135.45	<0.0001	significant
$x_3{}^2$	0.0001648	1	0.0001648	0.006433	0.95	0.3632	Not significant
Residuals	0.00122	7	0.0001742				
Loss of proposed item	0.00122	3	0.0004065				
Pure error	0.000	4	0.000				
Total	0.067	16					

Table 8. Reliability analysis of response surface model of the pressurization coefficient.

Mean	C.V. (%)	R^2	Adj R^2	Adeq Precision
0.75	1.76	0.9817	0.9582	17.842

The significance test of the regression equation was carried out through the analysis of variance, as shown in Table 7. Prob $(P) > F$ (P) in the table is the indicator of significant difference, and F is the test statistic, which is used for the analysis of variance. When P is less than 0.05, it indicates that the model fits well in the regression area, which is significant. When the Prob $(P) > F$ is less than 0.0001, the model fits well in the whole regression area and the test scheme is reasonable. In addition to the F test, R^2 and Adj R^2 can further verify the model's reliability. It is generally accepted that the larger the R^2 and Adj R^2, the better the regression model's fitting effect. R^2 and Adj R^2 in this model are 0.9817 and 0.9582, respectively, so the model fits well, and the prediction of the pressurization coefficient has high reliability. C.V. and Adeq precision can also be used to measure the reliability of the test. A small C.V. indicates that the test has good reliability and accuracy. The coefficient

of variation, C.V., of this model was 1.76%, indicating high test reliability. If the Adeq precision is greater than 4.0, it is considered that the test is reasonable. The Adeq precision of this model is 17.842, so the model test is feasible.

When the range of P is between 0 and 0.01, it is significant; when P ranges from 0.01 to 0.05, it is a secondary significant effect; when P is greater than 0.05, the effect is not significant. It can be seen from the table that the P values of x_1, x_2, x_3, x_1x_2, x_1x_3, x_2x_3, x_1^2, x_2^2 and x_3^2 are 0.8512, <0.0001, 0.0228, 0.4579, 0.3528, 0.388, 0.3424, <0.0001 and 0.3632, respectively. Therefore, groove depth $h(x_2)$ and groove number $z(x_3)$ are significant and secondary significant factors, respectively. In the square term, x_2^2 is a significant influencing factor.

3.1.2. Influence of Parameter Interaction on Pressurization Coefficient

In order to further determine the optimal value range of each design parameter, the three-dimensional response surface graph of each design parameter's interaction term was obtained using Design Expert. The three-dimensional response surface can present the regression function in the form of graphics, which can directly reflect the influence of design parameters on the response value and the interaction between design parameters.

(1) Through the calculation of the regression model, the response surface of the effect of the interaction term between groove width $b(x_1)$ and groove depth $h(x_2)$ on the pressurization coefficient φ^2 was generated when the coding level of groove number $z(x_3)$ was 0, as shown in Figure 5.
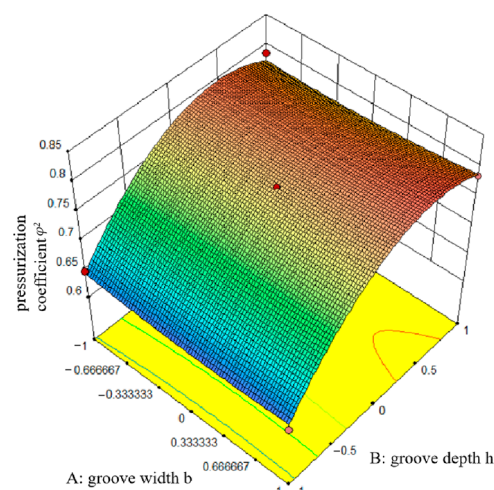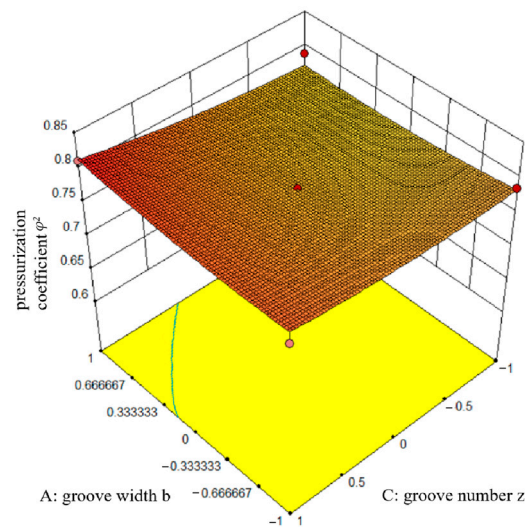

Figure 5. Effect of the interaction term between groove width and depth on the pressurization coefficient.

At a coding level of 0 for groove number z, the analysis of the effect of the interaction term between groove width b and groove depth h on the pressurization coefficient φ^2 reveals that the pressurization coefficient varies between approximately 0.65 and 0.8. The change in the pressurization coefficient φ^2 is not significant as the groove width gradually increases. In contrast, the effect of groove depth h on the standard pressurization coefficient φ^2 is more significant. When h is increased from coding level -1 to 0.8, the pressurization coefficient φ^2 increases gradually on the whole and decreases slightly near the coding level of 1. To sum up, to locate the pressurization coefficient in a better value range, the groove width interval should be 0.6 to 1. The groove depth interval should be selected as 0.25 to 0.8, which should be converted into the actual size parameters. Thus, the groove width interval is 12.8 mm to 14 mm, and the groove depth interval is 4.5 mm to 5.6 mm.

(2) Through the calculation of the regression model, the response surface of the effect of the interactive term of groove width $b(x_1)$ and groove number $z(x_3)$ on the pressur-

ization coefficient was generated when the coding level of $h(x_2)$ was 0, as shown in Figure 6.

Figure 6. Effect of the interaction term between groove width and number on the pressurization coefficient.

At a coding level of 0 for groove depth h, the analysis of the effect of the interaction term between groove width b and groove number z on the pressurization coefficient φ^2 reveals that the pressurization coefficient varies between approximately 0.78 and 0.81. The change in φ^2 is insignificant as the groove width gradually increases; with the increase in the groove number, the pressurization coefficient increases gradually. To sum up, to place the pressurization coefficient in a better value range, the groove width interval should be 0.15 to 1. The groove number interval should be 0.25 to 1, which should be converted into actual size parameters. That is, the groove width interval should be 11.45 mm–14 mm, and the groove number interval should be 23.5–28.

(3) Through the calculation of the regression model, the response surface of the effect of the interactive term of groove depth $h(x_2)$ and groove number $z(x_3)$ on the pressurization coefficient was generated when the coding level of groove width $b(x_1)$ was 0, as shown in Figure 7.
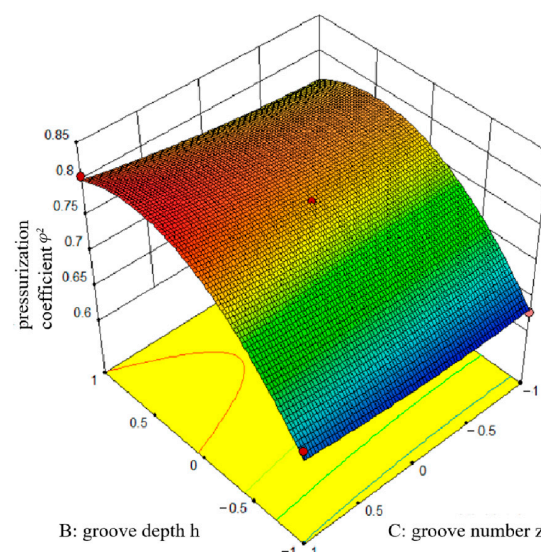
Figure 7. Effect of the interaction term between groove depth and number on pressurization coefficient.

The analysis of the effect of the interaction term between *h* and *z* on the pressurization coefficient φ^2 reveals that the pressurization coefficient varies between approximately 0.65 and 0.8. When the groove depth changes from coding level −1 to 1, the pressurization coefficient φ^2 gradually increases. Compared with the effect of the *h* on the pressurization coefficient, the effect of the *z* is relatively small. Therefore, to place the pressurization coefficient in a better value range, the groove depth interval should be 0.1–1. The groove number interval should be 0.25–1, which should be converted into actual size parameters. That is, the groove depth interval should be 4.2–6 mm, and the groove number interval should be 23.5–28.

Based on the above analysis of interaction term, to place the pressurization coefficient in a better value range, the groove width interval should be 12.8 mm to 14 mm; the groove depth interval should be 4.5 mm to 5.6 mm; and the groove number interval should be 23.5 to 28.

3.2. Results Analysis of Response Surface Optimization for Leakage Flow Rate

3.2.1. Parameter Significance Analysis

The leakage flow rate *Q* of the first-stage liquid-sealing impeller under each scheme is shown in Table 9.

Table 9. Numerical simulation results of the leakage flow rate.

Scheme	Y01	Y02	Y03	Y04	Y05	Y06
Q (kg/s)	19.15	16.946	16.77	12.68	19.48	17.06
Scheme	**Y07**	**Y08**	**Y09**	**Y10**	**Y11**	**Y12**
Q (kg/s)	14.89	12.22	19.30	17.39	16.52	12.75
Scheme	**Y13**	**Y14**	**Y15**	**Y16**	**Y17**	
Q (kg/s)	15.70	15.70	15.70	15.70	15.70	

Based on Design Expert 10.0, the response surface method was used to fit the numerical simulation results, and the regression equation of the leakage flow rate *Q* of the first-stage liquid-sealing impeller is as follows:

$$Q = 28.90608 - 0.31338x_1 - 0.11137x_2 - 0.28499x_3 - 0.07844x_1x_2 - \\ 0.00344x_1x_3 - 0.04525x_2x_3 + 0.010368x_1^2 + 0.14748x_2^2 + 0.00333x_3^2 \tag{6}$$

where x_1 is the groove width, x_2 is the groove depth, x_3 is the groove number, x_1x_2 is the interactive term of groove width and depth, x_1x_3 is the interactive item of groove width and number, and x_2x_3 is the interactive item of groove depth and number.

The results for the significance test of the regression equation coefficient and the reliability analysis of the response surface model are shown in Tables 10 and 11.

R^2 and Adj R^2 in this model are 0.9924 and 0.9826 respectively, indicating that the model has good fit and the prediction of leakage flow rate has high reliability; C.V. is 1.8%, indicating that the test has high reliability; and the accuracy of the model is 33.483, which shows that the model test scheme is feasible.

Through the significance test of regression equation coefficients, it can be seen that the *p* values of x_1, x_2, x_3, x_1x_2, x_1x_3, x_2x_3, x_1^2, x_2^2 and x_3^2 are <0.0001, <0.0001, <0.0001, 0.0142, 0.6823, 0.0072, 0.5304, 0.0042 and 0.4251, respectively. Therefore, the groove width $b(x_1)$, groove depth $h(x_2)$ and groove number $z(x_3)$ are all significant influencing factors. x_1x_3 and x_2x_3 are secondary significant influencing factors in the interactive term, and x_2^2 is a secondary significant influencing factor in the square term.

Table 10. Significance test of regression equation coefficient of the leakage flow rate.

Factor	Sum of Square	Degree of Freedom	Mean Square	Standard Deviation	F	Prob (P) > F	Significance
Model	78.73	9	8.53	0.13	101.29	<0.0001	significant
x_1	16.23	1	16.23	0.1	192.79	<0.0001	significant
x_2	19.97	1	19.97	0.1	237.25	<0.0001	significant
x_3	36.81	1	36.81	0.1	437.39	<0.0001	significant
$x_1.x_2$	0.89	1	0.89	0.15	10.53	0.0142	significant
$x_1.x_3$	0.015	1	0.015	0.15	0.18	0.6823	Not significant
$x_2.x_3$	1.18	1	1.18	0.15	14.02	0.0072	significant
x_1^2	0.037	1	0.037	0.14	0.44	0.5304	Not significant
x_2^2	1.47	1	1.47	0.14	17.41	0.0042	significant
x_3^2	0.06	1	0.06	0.14	0.72	0.4251	Not significant
Residuals	0.59	7	0.084				
Loss of proposed item	0.59	3	0.2				
Pure error	0.000	4	0.000				
Total	77.31	16					

Table 11. Reliability analysis of response surface model of the leakage flow rate.

Mean	C.V.%	R^2	Adj R^2	Adeq Precision
16.08	1.8	0.9924	0.9826	33.483

3.2.2. Influence of Parameter Interaction on Leakage Flow Rate

The three-dimensional response surface graph of each design parameter interaction item was analyzed in Design Expert, as shown in Figures 8–10.

(1) Through the calculation of the regression model, the effect of the interactive term of $b(x_1)$ and $h(x_2)$ on the leakage flow rate Q was generated when the coding level of $z(x_3)$ is 0. The response surface is shown in Figure 8.
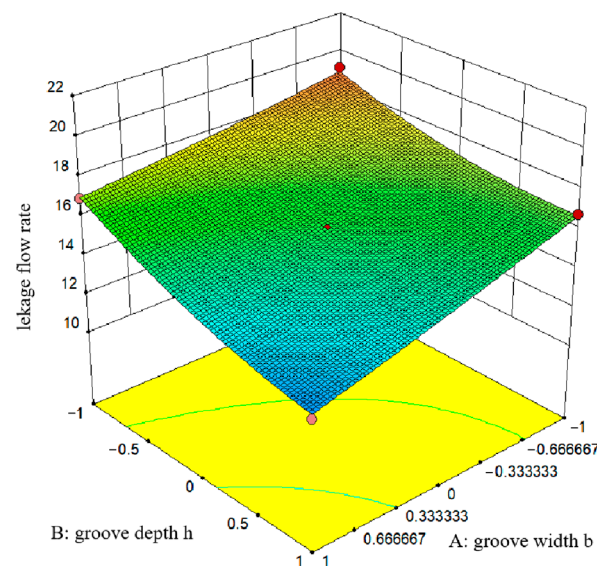
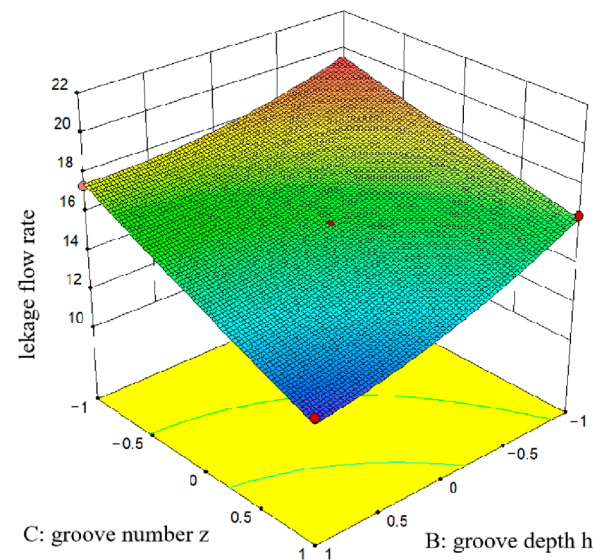**Figure 8.** Effect of the interaction term between groove width and depth on leakage flow rate.

When the coding level of groove number z is 0, through the analysis of the effect of the interactive terms of groove width b and groove depth h on the leakage flow rate Q, it is found that the leakage flow rate Q changes between 12 kg/s and 20 kg/s. Both groove width b and groove depth h have obvious effects on the leakage flow rate Q. When the b and h increase from coding level −1 to 1, the leakage flow rate Q gradually decreases. To sum up, to place the leakage flow rate in a better value range, the groove width interval should be 0.33–1. The groove depth interval should be 0.2–1, which should be converted

into actual size parameters. That is, the groove width interval should be 12 mm–14 mm, and the groove depth interval should be 4.4 mm–6 mm.

(2)   Through the calculation of the regression model, the effect of the interactive term of groove width $b(x_1)$ and groove number $z(x_3)$ on leakage flow rate Q was generated when the coding level of groove depth $h(x_2)$ is 0. The response surface is shown in Figure 9.
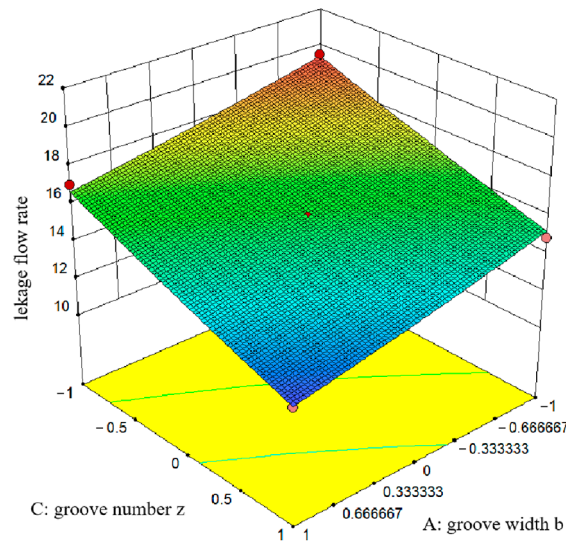
Figure 9. Effect of the interaction term of groove width and number on leakage flow rate.

Figure 10. Effect of the interaction term of groove depth and number on leakage flow rate.

When the coding level of groove depth h is 0, through the analysis of the effect of the interactive term of groove width b and groove number z on the leakage flow rate Q, it was found that the leakage flow rate Q changes between 14 kg/s and 18 kg/s. Both groove width b and groove number z have obvious effects on the leakage flow rate Q. When groove width b and groove depth h increase from coding level −1 to 1, the leakage flow rate Q gradually decreases. To sum up, to place the leakage flow rate in a better value range, the groove width interval should be −0.33–1. The groove number interval should be 0.15–1, which should be converted into actual size parameters; that is, the groove width interval should be 10 mm–14 mm, and the groove number interval should be 22.9–28.

(3) Through the calculation of the regression model, the effect of the interactive term of groove depth $h(x_2)$ and groove number $z(x_3)$ on the leakage flow rate Q was generated when the coding level of groove width $b(x_1)$ is 0. The response surface is shown in Figure 10.

When the coding level of groove width b is 0, through the analysis of the effect of the interactive term of groove depth h and groove number z on the leakage flow rate Q, it was found that the leakage flow rate Q changes between 14 kg/s and 18 kg/s. Both groove depth h and groove number z have obvious effects on the leakage flow rate Q. When groove depth h and groove number z increase from coding level -1 to 1, the leakage flow rate Q gradually decreases. To place the leakage flow rate in a better value range, the groove depth interval should be -0.2–1. The groove number interval should be 0.25–1, which should be converted into actual size parameters. The groove depth interval as such should be 3.6 mm–6 mm, and the groove number interval should be 23.5–28.

Based on the above analysis of the interaction term, to place the leakage flow rate in a better value range, the groove width interval should be 12–14 mm; the groove depth interval should be 4.4–6 mm; and the groove number interval should be 23.5–28.

To maximize the pressurization coefficient and minimize the leakage flow rate at the same time, the final value range of each parameter is: the groove width is 12.8 mm to 14 mm; the groove depth is 4.5 mm to 5.6 mm; and the groove number is 23.5 to 28.

3.3. Comparison of the Sealing Performance in the First-Stage Liquid-Sealing Impeller before and after Optimization

3.3.1. Determination of Optimization Scheme

In the previous section, the structural parameters of the first-stage liquid-sealing impeller were optimized using the response surface method, and the parameter value ranges that maximize the pressurization coefficient and minimize the leakage flow were determined, respectively. The parameter combination of groove width of 12.8 mm, groove depth of 4.5 mm and groove number of 24 was selected as the optimization scheme for numerical verification.

3.3.2. Comparison of Sealing Performance in the First-Stage Liquid-Sealing Impeller before and after Optimization

Three-dimensional modeling was carried out according to the optimized parameters. After optimization, the groove width b of the first-stage liquid-sealing impeller is 12.8 mm, the groove depth h is 4.5 mm, and the groove number z is 24. Other geometric parameters are consistent with the original model.

Figure 11 shows the flow field pressure distribution of the first-stage liquid-sealing impeller under the two schemes. Compared with the optimized scheme, the original scheme has lower pressure at the impeller inlet and more fluid entering the impeller. In the optimization scheme, due to the increase in the pressurization coefficient, the flow rate at the inlet of the impeller decreases, and the overall leakage flow rate also decreases. The pressure gradient at the groove's top and the groove's root inside the impeller are the most significant, and the high pressure is mainly distributed at the groove top and gradually decreases along the radial direction.

The combined velocity V_{YZ} nephogram in the YZ plane for the original and optimized model flow fields is given in Figure 12. It can be seen from the streamline that there is a large-scale vortex flow in both schemes. The impeller is closely related to the vortex flow in the flow channel or between the blades, so the appearance of the vortex positively improves the sealing performance. Under the same boundary conditions, the optimized scheme has a larger-scale vortex flow, which has a greater hindering effect on the gap between the impeller and the cavity, thereby achieving a better sealing effect.
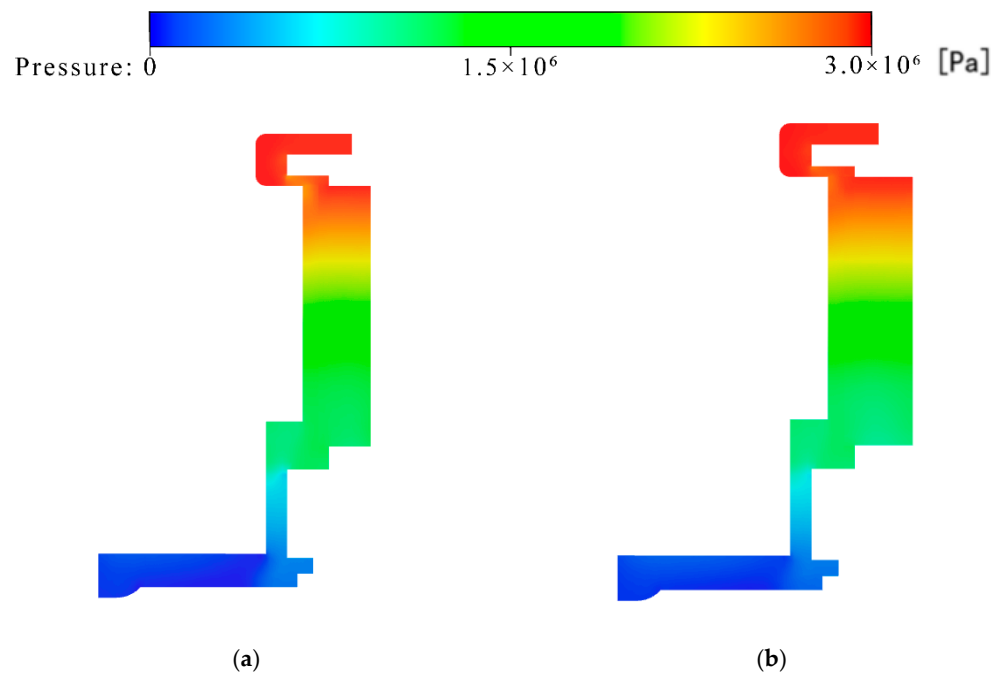
Figure 11. Comparison of pressure nephogram of different schemes. (**a**) Original model; (**b**) Optimized model.
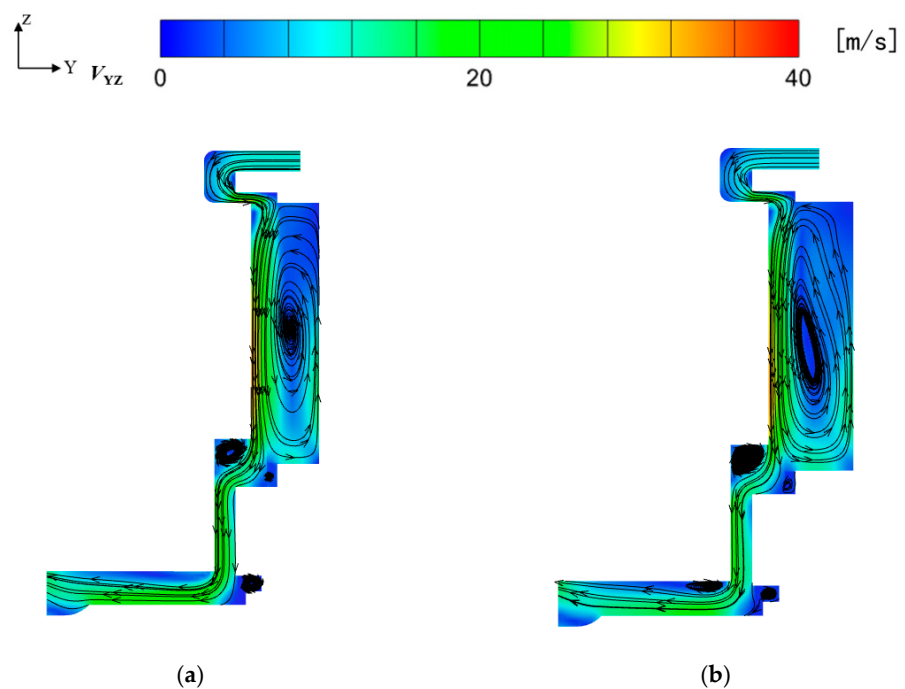
Figure 12. Comparison of velocity nephogram of different schemes. (**a**) Original model; (**b**) Optimized model.

The pressurization coefficient φ^2 and the leakage flow rate Q at each rotational speed were obtained and compared with the calculation results of the original model. The corresponding results are shown in Figures 13 and 14.
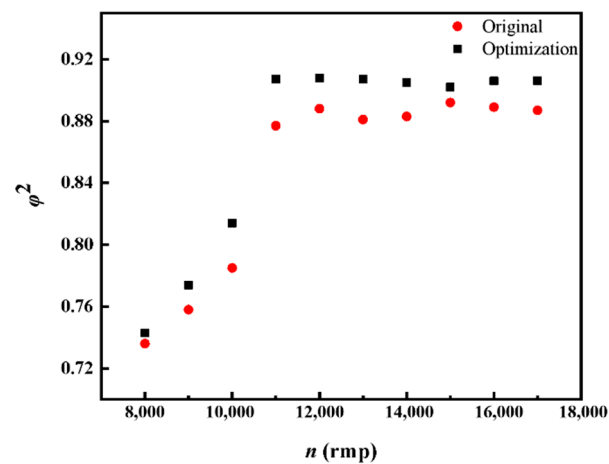
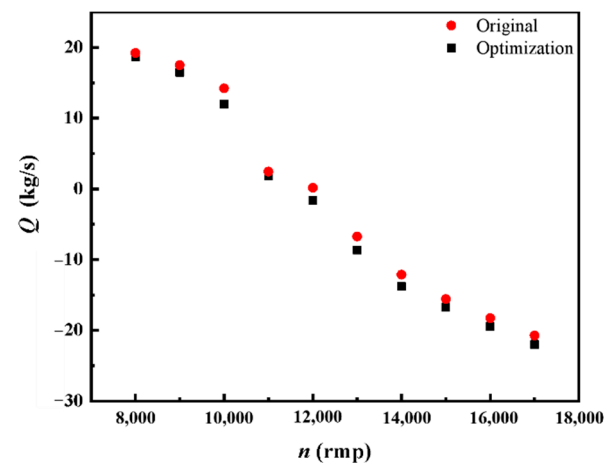**Figure 13.** Comparison of pressurization coefficient before and after optimization.

Figure 14. Comparison of leakage flow rate before and after optimization.

The comparison shows that the pressurization coefficient φ^2 of the optimized first-stage liquid-sealing impeller is increased at all speeds, with an average increase of 2.5%. Compared with the original model, the leakage flow rate of the optimized model decreases by an average of 8.2% in the leakage state. In the negative pressure sealing state, the reverse flow increases, with an average increase of 6.7%. Therefore, the optimization effect of the first-stage liquid-sealing impeller of the turbopump is obvious, which could be achieved through better sealing.

3.3.3. Numerical Calculation and Experimental Verification

To verify the accuracy of the numerical method, the sealing performance of the liquid sealing impeller before optimization was tested at the Xi'an Aerospace Power Research Institute. For safety reasons, the test uses liquid nitrogen as the working medium. During the test, the pressure data of monitoring point P26 were collected to test the first-stage liquid sealing impeller, as shown in Figure 15. At the same time, the numerical simulation results under liquid nitrogen are compared with the experimental data, as shown in Table 12. It can be seen from Table 12 that the numerical simulation results are close to the experimental results, and the deviations of the first and second upwind are 6.67% and 6.50%, respectively. Therefore, the numerical simulation method has a certain accuracy and can be used for subsequent research.
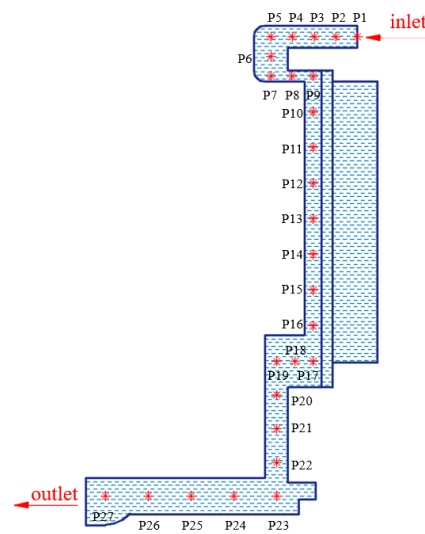
Figure 15. Schematic diagram of monitoring points.

Table 12. Comparison of numerical simulation results with experimental results.

Method	Pressure (MPa)	Relative Error (%)
Experimental values	0.18	
First-order upwind	0.168	6.67
Second-order upwind	0.1683	6.50
Method	**Flow Rate (kg/s)**	**Relative Error (%)**
Experimental values	12.09	
First-order upwind	11.15	7.78
Second-order upwind	11.20	7.36

4. Conclusions

In this paper, the structure of a first-stage liquid-sealing impeller of a turbopump was optimized, and the regression equation of three structural parameters, pressurization coefficient φ^2; leakage flow rate Q; and groove width b, groove depth h and groove number z was established using the response surface method. The influence law of each parameter on the pressurization coefficient φ^2 and the leakage flow rate Q was analyzed, and the optimized parameter interval was obtained. A set of parameter combinations was selected as the optimization scheme in the interval, and the optimized model was simulated and compared with the original model. The conclusions follow.

(1) For the pressurization coefficient, within the selected range: the larger the groove width b, the larger the pressurization coefficient; within the variation range of groove depth h, the optimal interval of pressurization coefficient exists; the larger the number of groove z, the larger the pressurization coefficient. For the leakage flow rate, in the selected range: the smaller the groove width b, the smaller the leakage flow rate; the smaller the groove depth h, the smaller the leakage flow rate; and the smaller the number of groove z, the smaller the leakage flow rate. However, in practical application, the problem of mutual interference between grooves should be considered when the groove width and the number of grooves increase.

(2) Groove width b, groove depth h and groove number z have different degrees of influence on the pressurization coefficient and the leakage flow rate of the first-stage liquid-sealing impeller. In order to make the pressurization coefficient larger and the leakage flow smaller at the same time, the value ranges of the groove width b,

groove depth *h* and groove number *z* should be 12.8–14 mm, 4.5–5.6 mm and 23.5–28, respectively.

(3) Taking the groove width *b* as 12.8 mm, the groove depth as 4.5 mm, and the groove number *z* as 24 as the optimization scheme for numerical calculation, the results show that compared with the original scheme, the pressurization coefficient φ^2 of the optimization model increased by 2.5% on average at each speed. The leakage flow rate *Q* reduced by 8.2% on average in the leakage state. In the negative pressure sealing state, the reverse flow rate *Q* increased by 6.7% on average, realizing the optimization effect.

References

1. Wolf, J.E.; Connelly, R.E. Development of Seals for Rocket Engine Turbopumps. *ASLE Trans.* **1959**, *2*, 25–31. [CrossRef]
2. Masataka, N.; Wang, J.Y. Research on Trial Production of Seals for Liquid Hydrogen Turbopumps. *Missiles Space Veh.* **1982**, *11*, 29–36.
3. Zhang, B.L. Several Problems of High-Speed Turbopump. *J. Astronaut.* **1983**, *4*, 81–90.
4. Dirusso, E. Design Analysis of a Self-Acting Spiral-groove Ring Seal for Counter-rotating Shafts. In Proceedings of the 19th Joint Propulsion Conference, Seattle, WA, USA, 27–29 June 1983. [CrossRef]
5. Du, T.E. New Sealing Structure of High-Pressure Liquid Rocket Engine. *J. Propuls. Technol.* **2000**, *21*, 16–19. [CrossRef]
6. Huang, Z.Y.; Li, H.M.; Hu, Z.B. Study on Floating Seal Ring of Hyper-rotate-speed Pump in Liquid Rocket Engine. *J. Rocket Propuls.* **2004**, *30*, 10–14. [CrossRef]
7. Lee, Y.B.; Kim, K.W.; Ryu, S.J.; Chung, J.T. Leakage Performance and Rotordynamic Characteristics of Bump Floating Ring Seals for Turbopump. In Proceedings of the ASME Turbo Expo: Turbine Technical Conference and Exposition, Dusseldorf, Germany, 16–20 June 2014. [CrossRef]
8. Huang, F.L. Research on Dynamic Characteristics of Liquid Hydrogen Turbopump Rotor-Seal System. Master's Thesis, Harbin Institute of Technology, Harbin, China, 2014. [CrossRef]
9. Zhang, S.Q.; Chen, J.; Zhao, W.G.; Wang, L. Research Status and Prospect of Non-Contact Seal for Liquid Rocket Engine Turbopump. In Proceedings of the 1st JCAP and 37th APTIS Technical Conference, Xi'an, China, 17 August 2016; Available online: https://d.wanfangdata.com.cn/conference/ChZDb25mZXJlbmNlTmV3UzIwMjIwOTAxEhVIWUMyMDE2MTIyOTAwMDAwMDI4NjMaCDI0em9ia3Yy (accessed on 30 September 2021).
10. Zhao, W.G.; Zhang, S.Q.; Chen, J.; Wang, L. Key Technologies of Dynamic-hydrostatic Hybrid Seals Used in Liquid Oxygen Pump. *Lubr. Eng.* **2017**, *42*, 111–115. [CrossRef]
11. Zhuang, S.G.; Song, Y.; Yang, X.H.; Wang, L. The Flow Characteristics Study of Floating Ring Seal of Liquid Rocket Engine. In Proceedings of the 2nd JCAP and 38th APTIS Technical Conference, Dalian, China, 23 August 2017; Available online: https://kns.cnki.net/kcms/detail/detail.aspx?FileName=HTDZ201708001001&DbName=CPFD2017 (accessed on 23 November 2021).
12. Wei, F.S.; Xie, Q.; Qi, P.J.J.; Dong, F.; Wang, L. Computation and Experimental Research of Face Seal off Pressure for Liquid Rocket Engine. *Aerosp. Manuf. Technol.* **2019**, *4*, 27–30. [CrossRef]
13. Xu, L.S.; Wu, J.H.; Wang, Y.L.; Rafique, F.; Xu, J.M.; Yuan, X.Y. Lubrication and Stability Enhancement by Attaching Superconducting Magnetic Force on Non-contacting Mechanical Seals for Reusable Rocket Turbopump. *Proc. Inst. Mech. Eng. Part J-J. Eng. Tribol.* **2021**, *236*, 892–907. [CrossRef]
14. Zhuang, S.G.; Bao, H.F.; He, Z.F.F.; Wang, K.; Liu, H.L. The Influence of Rotating Speed on the Sealing Characteristics of a Liquid-Sealing Impeller for a Liquid Oxygen Turbopump. *Processes* **2022**, *10*, 1366. [CrossRef]
15. Box, G.E.P.; Wilson, K.B. On the Experimental Attainment of Optimum Conditions. *J. R. Stat. Soc.* **1951**, *13*, 1–45. [CrossRef]

16. Ferreira, S.L.C.; Bruns, R.E.; Ferreira, H.S.; Matos, G.D.; David, J.M.; Brandão, G.C.; Da-Silva, E.G.P.; Portugal, L.A.; Dos-Reis, P.S.; Souza, A.S.; et al. Box-Behnken Design: An Alternative for the Optimization of Analytical Methods. *Anal. Chim. Acta* **2007**, *597*, 179–186. [CrossRef] [PubMed]

17. Rahimi, M.; Valeh-e-Sheyda, P.; Rashidi, H. Statistical Optimization of Curcumin Nanosuspension Through Liquid Anti-solvent Precipitation (lasp) Process in a Microfluidic Platform: Box-behnken Design Approach. *Korean J. Chem. Eng.* **2017**, *34*, 3017–3027. [CrossRef]